ORIGINAL PAPER

Comparative NMR Relaxivity Study of Polyoxometalate-Based Clusters $[Mn_4(H_2O)_2(P_2W_{15}O_{56})_2]^{16-}$ and $[\{Dy(H_2O)_6\}_2Mn_4(H_2O)_2(P_2W_{15}O_{56})_2]^{10-}$ from 20 MHz to 1.2 GHz

Masooma Ibrahim, et al. *[full author details at the end of the article]*

Abstract

Nuclear Magnetic Resonance relaxivities are a measure for the sensitivity of a contrast agent (CA), i.e. the potential of a paramagnetic moiety to enhance longitudinal and transverse relaxation of molecules in its near neighbourhood. The underlying mechanism is called Paramagnetic Relaxation Enhancement (PRE). The relaxivity, characterizing PRE, depends not only on the external applied magnetic field but also depends on numerous factors, such as number of coordinated water molecules, water exchange rate, rotational diffusion, first and second coordination hydration sphere, electronic and magnetic properties of paramagnetic centers and the molecular shape/ size of the CA. Relaxation rates are usually normalized to the concentration of the contrast agent to provide the relaxivities. To investigate the influence of these factors on PRE of newly synthesized potential CA, two paramagnetic metals containing polyoxometalates (POMs) $[Mn_4(H_2O)_2(P_2W_{15}O_{56})_2]^{16-}$ (**Mn$_4$-P$_2$W$_{15}$**) and $[\{Dy(H_2O)_6\}_2Mn_4(H_2O)_2(P_2W_{15}O_{56})_2]^{10-}$ (**Dy$_2$Mn$_4$-P$_2$W$_{15}$**) were selected as models to be studied at ^{1}H Larmor frequencies from 20 MHz to 1.2 GHz. Structurally, the POM **Dy$_2$Mn$_4$-P$_2$W$_{15}$** is similar to the tetra-nuclear manganese(II)-substituted sandwich-type POM **Mn$_4$-P$_2$W$_{15}$**, with the two coordinated Dy^{III} cations acting as linkers connecting **Mn$_4$-P$_2$W$_{15}$** units, thus forming a 1D ladder-like chain structure based on sandwich-type rungs strung together by the dysprosium cations. This study shows that POM (**Dy$_2$Mn$_4$-P$_2$W$_{15}$**) is a promising CA at high magnetic fields and proves that the use of heterometallic clusters is an effective strategy to increase PRE due to the synergistic effects from different metal ions.

✉ Gisela Guthausen
   gisela.guthausen@kit.edu

✉ Annie K. Powell
   annie.powell@kit.edu

Extended author information available on the last page of the article

1 Introduction

Nuclear Magnetic Resonance (NMR) contrast agents are characterized by their Paramagnetic Relaxation Enhancement (PRE). PRE is the degree to which the paramagnetic molecules/contrast agents can enhance the longitudinal and transverse relaxation rates ($R_1 = 1/T_1$ and $R_2 = 1/T_2$, respectively) of molecules in their nearest surroundings. This phenomenon occurs due to fluctuating hyperfine interactions between the unpaired electrons of a paramagnetic ion and the surrounding molecules, usually water. A major challenge of Magnetic Resonance Imaging (MRI) is its relatively low sensitivity, therefore, a considerable amount of effort is directed towards creating new contrast agents for improved sensitivity and image contrast. As the sensitivity of NMR/MRI increases with magnetic field due to increased polarization, a trend in NMR/MRI research is to use higher fields. Until recently, most clinical MRI scanners operate at 3 T; however, higher magnetic fields up to 9.4 T have been used under appropriate ethical agreement for neuroscientific and clinical research since the late 1990s. However, there are still technological, physical and safety limitations at high magnetic fields [1–4]. The drive toward higher field strengths is also important for the purpose of fundamental research, for material science and for industrial applications (imaging of non-living objects for quality assurance and inspection). MRI is finding increasing applications in various areas, such as water treatment, petrogeology, medical implants, food, agriculture, polymers and polymer composites, and pharmaceuticals. Perhaps the most eminent advantage in applying magnetic resonance methods in chemical engineering research is that both chemistry and transport can be tracked in three dimensions in optically opaque systems [5, 6]. Gd^{III} containing compounds are well known for their T_1 relaxation enhancing capability due to its isotropic electronic ground state ($^8S_{7/2}$) and long electronic relaxation time (τ_S). However, the r_1 relaxivity often decreases with magnetic field for most of the well-known and established contrast agents [7]. This behavior represents a challenge for current contrast agent design. Therefore, it is important to develop new high-field contrast agents for emerging high-field MRI applications in medicine as well as in chemical engineering systems. In fact, recent research has shown that paramagnetic lanthanide ions, such as dysprosium(III), due to its asymmetric/anisotropic electronic ground state ($^6H_{15/2}$), short electronic relaxation time ($\sim 10^{-13}$ s) and a very high magnetic moment ($\mu = 10.2$ µB) has the tendency to exhibit especially a high transverse relaxivities at high magnetic fields, this makes Dy^{III} based compounds promising candidate for dominantly T_2 contrast enhancement at ultra-high fields [8–10]. In some compounds also the Dy^{III} longitudinal relaxivities increase with field, which is the preferred contrast enhancement.

Relaxivity depends not only on the field and on the intrinsic electronic properties of the paramagnetic centers but also on the temperature, molecular mobility, the number of exchangeable water molecules and their distance to paramagnetic centers as well as their rate of exchange with bulk solvent [11]. Concerning adjustment of dose or concentration, new classes of contrast agents with improved relaxivity can be designed by incorporating high numbers of

paramagnetic centers within the same molecule or cluster that in turn means that lower doses can be given to produce marked alterations in contrast [7, 12]. Up till now, the NMR relaxivities of ultra-high ground spin state cyclic coordination clusters based on 3d and 4f ions $[Fe^{III}_{10}Ln^{III}_{10}(Me\text{-}tea)_{10}(Me\text{-}teaH)_{10}(NO_3)_{10}]$ (Ln = Dy, Gd; Me-tea = triethanolamine) were studied over a wide range of ^1H Larmor frequencies from 10 MHz up to 1.4 GHz [13, 14] and the PRE properties of polyoxometalate (POM) clusters containing both 3d and 4f paramagnetic ions $\{Ln_{30}Co_8Ge_{12}W_{108}O_{408}\}$ $\{Ln_{30}Co_8\}(Ln = Gd, Dy)$ were studied as well up to 1.4 GHz [15]. These investigations revealed that the relaxivities of these clusters containing a large number of paramagnetic centers are in sum much higher than the commercially available, often Gd-based medical contrast agents with only one paramagnetic center. Polyoxometalate (POM) clusters represent a class of inorganic compounds, which show an unmatched variety of molecular and electronic structures with unique properties that make them attractive for applications in magnetism, magnetic coolers, imaging, catalysis, energy and medicine [15–20]. Although a wide range of biological activities of POMs have been reported, their broad-spectrum interactions with biomolecules and toxicity hinder their clinical usage [19]. Concerning non-medical applications, POMs possess high potential to be used as industrial contrast agents due to the low cost synthesis, stability, solubility and robust nature. POMs and their lacunary derivatives can be functionalized by grafting of the organic substituents and metal cations onto the surface, which offers the possibility to fine-tune the properties of the resulting hybrid system. Under controlled basic conditions, lacunary POM ligands can be produced by removing one or more metal-oxo polyhedra from the parent POM structures. Lacunary POMs offer unique features as ligands, including their size, diamagnetic nature, arrangement of coordination sites, flexibility of coordination modes and ability to rearrange, making it possible to incorporate any number of 3d-paramagnetic metal centers [21, 22], lanthanide ions [23, 24], 3d-4f-metal ions [15, 17, 25] and organic groups [26].

In this work, two POM compounds $Na_{16}[Mn_4(H_2O)_2(P_2W_{15}O_{56})_2]\cdot53H_2O$ (shortened to **$Mn_4\text{-}P_2W_{15}$**) [27] and $Na_{10}[\{Dy(H_2O)_6\}_2Mn_4(H_2O)_2(P_2W_{15}O_{56})_2]\cdot59H_2O$ (shortened to **$Dy_2Mn_4\text{-}P_2W_{15}$**) [28] were selected as models to be examined for their PRE at ^1H Larmor frequencies from 20 MHz to 1.2 GHz.

1.1 Structure of the POMs

$Mn_4\text{-}P_2W_{15}$ is constructed by two trilacunary POM ligands $[P_2W_{15}O_{56}]^{12-}$ sandwiching a tetra-nuclear Mn cluster $\{Mn_4O_{16}(H_2O)_2\}$ (4 paramagnetic Mn^{II} ions with electron spin $S = 5/2$) through the W–O–Mn and P–O–Mn bridging modes. There are two terminal / exchangeable water molecules that are directly attached to the paramagnetic cluster $\{Mn_4O_{16}(H_2O)_2\}$ (Fig. 1). The **$Dy_2Mn_4\text{-}P_2W_{15}$** compound consists of a **$Mn_4\text{-}P_2W_{15}$** unit and two Dy^{III} metal ions (2 paramagnetic Dy^{III} ions with $S = 5/2$) attached to the POM skeleton (Fig. 2). Each Dy^{III} center connects two **$Mn_4\text{-}P_2W_{15}$** subunits via two W=O···Dy bonds forming a one-dimensional (1D) ladder-like chain, built up of the sandwich anions **$Mn_4\text{-}P_2W_{15}$** and the Dy^{III} ions (Fig. 3).
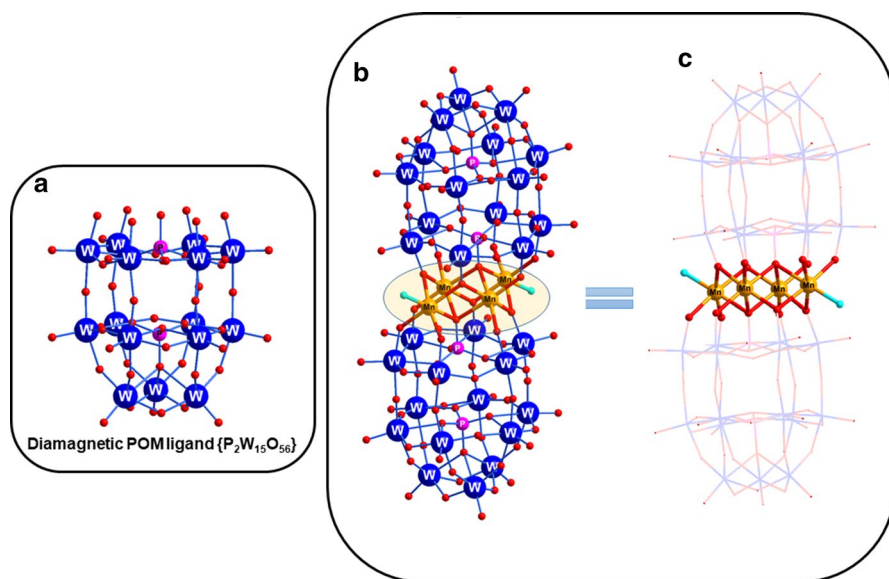
Fig. 1 Ball-and-stick and wire representation for crystal structure of Mn_4-P_2W_{15}: **a** Diamagnetic POM ligand $\{P_2W_{15}O_{56}\}$. **b** Compound Mn_4-P_2W_{15}. The paramagnetic $\{Mn_4\}$ core is highlighted in colour. **c** Compound Mn_4-P_2W_{15} where POM ligands are shown in wire-and-stick representation. For clarity, cation and crystal water molecules are omitted. Colour code: Oxygen = red balls, aqua ligand on Mn ions = turquoise balls (colour figure online)
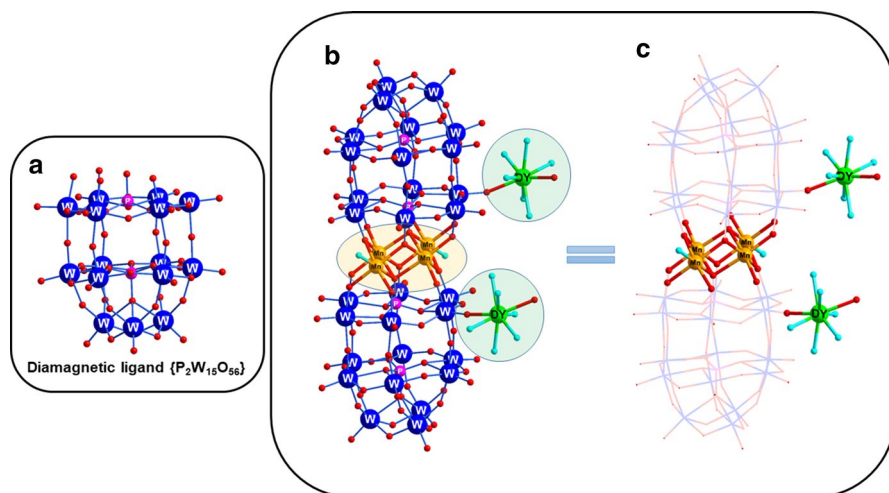

Fig. 2 Ball-and-stick and wire representation for crystal structure of Dy_2Mn_4-P_2W_{15}: **a** Diamagnetic POM ligand $\{P_2W_{15}O_{56}\}$. **b** Compound Dy_2Mn_4-P_2W_{15}. The paramagnetic $\{Mn_4\}$ core and Dy metal ions attached to the POM skeleton are highlighted in colours. **c** Compound Dy_2Mn_4-P_2W_{15} where POM ligands are shown in wire-and-stick representation. For clarity, cation and crystal water molecules are omitted. Colour code: Oxygen = red balls, aqua ligand on Dy and Mn ions = turquoise balls (colour figure online)
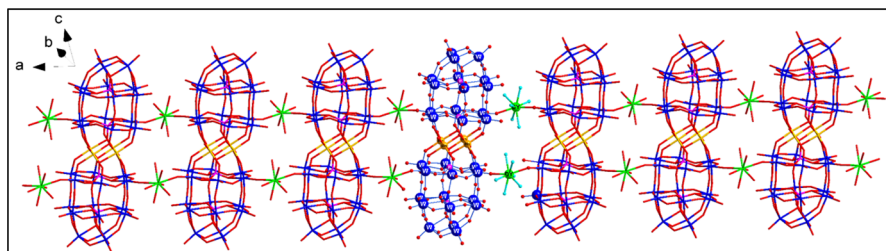
Fig. 3 Ball-and-stick representation for crystal structure of **Dy$_2$Mn$_4$-P$_2$W$_{15}$** as the 1D ladder-like chain with other units shown in wire-and-stick representation for clarity. Colour code: Oxygen = red balls, aqua ligand on Dy metal ions = turquoise balls (colour figure online)

The paramagnetic centers {Dy(H$_2$O)$_6$} and {Mn$_4$(H$_2$O)$_2$} in **Dy$_2$Mn$_4$-P$_2$W$_{15}$** have 6 and 2 directly coordinated exchangeable water molecules, respectively (Fig. 2). The terminal water ligands connected to the metal cations are labile enough to be potentially exchangeable by solvent water molecules or any organic substrates present in the solution [26]. The Dy^{III} metal ions remain attached to the POM skeleton in aqueous solution as shown by photoluminescence studies. More details about these solution studies are reported in [28], where, however, the existence of a 1D structure in solution could not be identified. The sodium cations can allow further growth of the crystal structure into a 2D framework. Such structures, constructed from alkali metal cation linkers, usually collapse in solution due to the weak interactions as established from mass spectroscopy studies on extended POM frameworks [Ln(H$_2$O)$_n$GeW$_{11}$O$_{39}$]$^{5-}$ (Ln = Dy, Er; n = 4, 3) [29].

1.2 Magnetic Properties

Magnetic properties of the POMs **Mn$_4$-P$_2$W$_{15}$** and **Dy$_2$Mn$_4$-P$_2$W$_{15}$** have also been reported [28]. The room temperature $\chi_M T$ product (χ_M = molar magnetic susceptibility) for **Mn$_4$-P$_2$W$_{15}$** is close to the expected value for four isolated Mn^{II} ions, 16.8 cm^3 K mol^{-1} (cf. 17.5 cm^3 K mol^{-1} for four Mn^{II}, electron spin s = 5/2, gyromagnetic ratio g = 2.00). Furthermore, molar magnetization (M_β) at 2 and 5 K as function of applied magnetic field in the range 0–7 T indicates a strong anti-ferromagnetic interaction. The temperature-dependent product $\chi_M T$ of **Dy$_2$Mn$_4$-P$_2$W$_{15}$** displays a room temperature $\chi_M T$ value of 45.3 cm^3 K mol^{-1} close to the expected value for four isolated Mn^{II} ions and two non-interacting Dy^{III}, 45.8 cm^3 K mol^{-1} for four Mn^{II}, s = 5/2, g = 2.00 and two Dy^{III}, S = 5/2; g_J = 4/3). The collective effects of the anti-ferromagnetic exchange operating in the **Mn$_4$-P$_2$W$_{15}$** unit along with the anisotropic magnetic properties of Dy^{III} ions have been observed in **Dy$_2$Mn$_4$-P$_2$W$_{15}$**. $M_\beta(H)$ for compound **Dy$_2$Mn$_4$-P$_2$W$_{15}$** displays very anisotropic behaviour and no saturation of the magnetization is observed. More details about synthesis, structure, characterization, and magnetic studies are reported in [28]. These two POMs with different structural compositions which remain intact in solution provide suitable systems to carry out comparative PRE studies to check the influence of Dy^{III} ions and size effects under various applied magnetic fields, i.e. ^{1}H Larmor frequencies.

2 Results and Discussion

Water is the prominent solvent in biological and medical CA applications and it is also common in chemical and process engineering. One way to design CAs for MRI with suitable parameters at high magnetic fields and knowing the behaviour of the presented POMs in aqueous solutions are essential. Both compounds **Mn$_4$-P$_2$W$_{15}$** and **Dy$_2$Mn$_4$-P$_2$W$_{15}$** are soluble and stable in aqueous media. The equimolar clear solution of POM **Dy$_2$Mn$_4$-P$_2$W$_{15}$** resulted through sonication, whereas the clear solution of the POM **Mn$_4$-P$_2$W$_{15}$** was obtained on stirring. It has always been great challenge to understand the complicated solution behaviour of large POM clusters. Contrary to what might be expected, large highly charged particles are known to form large agglomerations in diluted aqueous systems. Many types of giant POMs (macroanions) are hydrophilic and very soluble in water or other polar solvents because of the external water ligand layer and the negative charges of the POMs, which are balanced by small counterions, such as Na$^+$, Li$^+$, K$^+$ and NH$_4^+$. Such hydrophilic macroanions tend to self-assemble further into hollow, spherical, single-layer "blackberry"-type structures mostly in very dilute solution ($< 1 \times 10^{-5}$ mol L^{-1}). Generally, in polyoxometalate chemistry, the aggregation process is termed as blackberry formation, which is different from the aggregation of hydrophobic colloids forming through van der Waals forces, which leads to phase separation. This unique solution behaviour of POMs can be investigated by a combination of application of laser light scattering (LLS), dynamic light scattering (DLS), small angle X-ray scattering (SAXS), and small angle neutron scattering (SANS). In the present study, the blackberry formation is unlikely because blackberry structures are not easy to form due to the high-energy barrier between discrete single macroanions and supramolecular structures. There are different parameters (variation of solvent mixture/concentration/pH/time) that need to be optimized for the formation of blackberries [30]. During the PRE measurements, also at the highest Larmor frequency, no agglomeration was observed in the small cylindrical volumes of 1 mm in diameter, 1–2 mm in height (> 400 MHz).

2.1 PRE: Paramagnetic Relaxation Enhancement

Having shown the basic suitability of the POMs to serve as CA in aqueous solutions, the dispersion of the longitudinal and the transverse relaxivities were investigated while the ^{1}H Larmor frequencies ν_0 corresponding to magnetic fields ranged from 20 MHz up to 1.2 GHz in the present study. The experimental details of the NMR measurements have been described previously in detail in [13–15]. Essentially, NMR systems based on permanent magnets (≤ 80 MHz), on superconducting magnets (≤ 400 MHz) and on high-power (24 MW) electromagnets (≥ 800 MHz) were used to measure the relaxivities of the POMs. Inversion recovery and CPMG multi-echo sequences were applied to measure relaxation rates R_1 and R_2 as function of concentration in 0.2 mM steps over the range 0–1 mM at each magnetic field. The rates depend linearly on concentration as expected for a homogeneous solution

where aggregation especially at the larger concentrations does not play an important role. Therefore, the data were condensed to the plot of both relaxivity dispersions being discussed below. The coefficients of determination were in the range [0.95;0.9998] for the linear regressions for obtaining the relaxivities from the concentration dependent relaxation rates.

2.1.1 Inner Sphere (IS) and Outer Sphere (OS) Contribution

The paramagnetic relaxation in the present study can be explained by intermolecular dynamics of the water molecule with respect to the contrast agents. The basis is the hyperfine interaction between ^{1}H spins and the electronic spins of the paramagnetic ions. Diverse influencing factors are known which need to be quantified when aiming for a theoretical explanation of the observed PRE. For a detailed description, we refer to the book by Bertini et al., where the theoretical framework of PRE is given [31]. The Solomon–Bloembergen–Morgan theory, as well as the Curie spin approach, isotropic and dipolar contributions, is described there. In this article, we restrict ourselves to the following rough picture: The PRE phenomena are split into the inner sphere (IS) and outer sphere (OS) contributions for simplicity. The inner sphere (metal-bound) contribution comes from the nuclear spins (usually ^{1}H)/water molecules directly attached to the paramagnetic centers in the complex. The outer sphere contributions roughly correspond to the relative translational and rotational Brownian motions of free water molecules (bulk water molecules in the nearby environment) with respect to paramagnetic centers [32].

2.1.2 Longitudinal Relaxivity r_1

Both POMs show PRE as expected due to the presence of paramagnetic centers in the clusters (Fig. 4). In the case of $\mathbf{Dy_2Mn_4}$-$\mathbf{P_2W_{15}}$, the longitudinal relaxivities r_1 are larger compared to $\mathbf{Mn_4}$-$\mathbf{P_2W_{15}}$ which can be attributed to the electron spin effect of the two Dy^{III} and four Mn^{II} ion compared to the electron spin effect of four Mn^{II} ions in $\mathbf{Mn_4}$-$\mathbf{P_2W_{15}}$. Assuming that the electron spins of the individual ions add up in the cluster, the total electron spin would be 15 in $\mathbf{Dy_2Mn_4}$-$\mathbf{P_2W_{15}}$ and 10 in $\mathbf{Mn_4}$-$\mathbf{P_2W_{15}}$ leading to an expected increase of PRE by a factor in the order of 1.5 using this simplistic approach of assuming that the cluster effectively acts as one single moiety in PRE, i.e. that the effective, total spin accounts for the observed PRE. We experimentally observe a factor in the order of 4 between $\mathbf{Dy_2Mn_4}$-$\mathbf{P_2W_{15}}$ and $\mathbf{Mn_4}$-$\mathbf{P_2W_{15}}$. This is a strong indication that the simple picture is not appropriate. As seen in the chemical structure, the Dy ions are surrounded by water molecules, and it is very likely that chemical exchange occurs. In a theoretical description of PRE of these POMs, inner sphere contributions are, therefore, likely to be considered for PRE introduced by the Dy ions, whereas the Mn ions seem to contribute to PRE dominantly by outer sphere contributions. Additionally, the rotational correlation times will be different for $\mathbf{Dy_2Mn_4}$-$\mathbf{P_2W_{15}}$ and $\mathbf{Mn_4}$-$\mathbf{P_2W_{15}}$.

For application as a CA, a high r_1 is especially desirable as the reduction of longitudinal relaxation leads to a positive contrast enhancement in MRI. In addition, a high PRE allows reduction concentration in the making MRI less invasive in total.

However often, r_1 decreases with magnetic field. This is not the case for the ultra-high magnetic clusters {$Dy_{30}Co_8$} and {$Fe_{10}Dy_{10}$} already described in our papers [13–15]. There we found that these Gd clusters show a slight decrease of r_1 while the Dy analogues show an increase with Larmor frequency. Here, r_1 is found to be field independent or to slightly increase within the experimental error for **Dy$_2$Mn$_4$-P$_2$W$_{15}$** (Fig. 4). As discussed in previous publications, cooperative effects as well as the electronic correlation times must be considered and in the present case, chemical exchange and inner sphere contributions need to be considered.

2.1.3 Transverse Relaxivity r_2

Not only the longitudinal but also the transverse relaxivities are of importance in the application of a magnetic cluster as CA. Most of the MRI pulse sequences are based on either gradient or spin echoes leading to a non-negligible influence of transverse relaxation. The values of r_2 are usually much larger than r_1, while increasing with magnetic field. Again, r_2 is larger for **Dy$_2$Mn$_4$-P$_2$W$_{15}$** making the significance of the Dy ions evident (Fig. 5). Similar findings were made for {$Dy_{30}Co_8$}[15]. As usual, the relaxivity increases, in the present case approximately linearly, with field, leading to an enhanced negative image contrast at larger fields. Influencing factors again are—apart from the electronic correlation times—the rotational and diffusional correlation times as well as the chemical exchange probability which is enhanced for **Dy$_2$Mn$_4$-P$_2$W$_{15}$** compared to **Mn$_4$-P$_2$W$_{15}$**. Please also note that the exposure of water molecules in the surrounding of the Dy ions is much more pronounced than that of the Mn ions leading to the drastic enhancements in the case of **Dy$_2$Mn$_4$-P$_2$W$_{15}$** compared to **Mn$_4$-P$_2$W$_{15}$**. In fact, the transverse relaxivities of both compounds are much larger than the longitudinal relaxivities. This means that the POMs studied here are dominantly r_2 or "negative" relaxation agents. However, they should not be considered as superparamagnetic particles as the chemical structure and the physical mechanism differ considerably. This is evident in the case of exchangeable water molecules discussed above (Figs. 1 and 2).

Fig. 4 Longitudinal relaxivities r_1 of the total clusters as a function of ^{1}H Larmor frequency. Both POMs show PRE reflecting the contributions of Mn^{III} and Dy^{III}
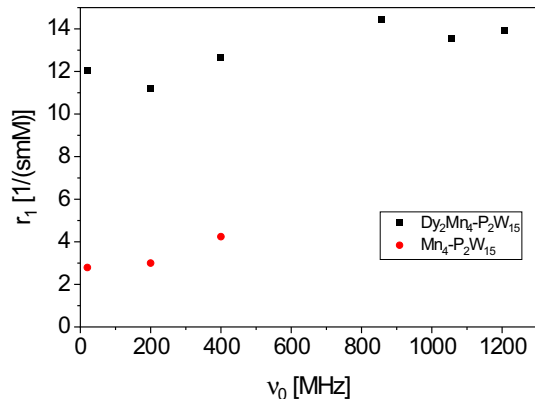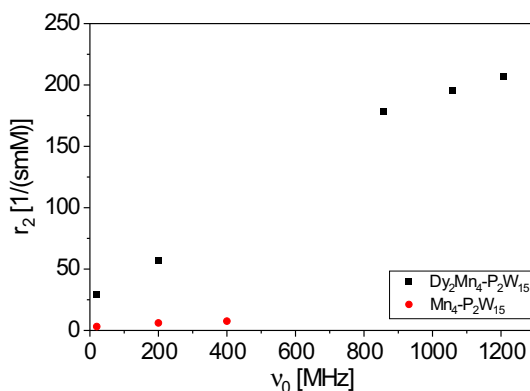
Fig. 5 As in Fig. 4 for longitudinal relaxivity, the values of transverse relaxivity are clearly lower for Mn_4-P_2W_{15}. Please note additionally the approximately linear increase of r_2 with Larmor frequency for Dy_2Mn_4-P_2W_{15}

3 Materials and Methods

The compounds $Na_{16}[Mn_4(H_2O)_2(P_2W_{15}O_{56})_2]0.53H_2O$ [27] and $Na_{10}[\{Dy(H_2O)_6\}_2Mn_4(H_2O)_2(P_2W_{15}O_{56})_2]\cdot59H_2O$ [28] were synthesized according to the literature methods and were characterized by IR spectroscopy. All reactions were carried out under aerobic conditions. All other reagents were purchased commercially and were used without further purification.

4 Conclusion

Herein we have presented the PRE properties of two POM clusters **Mn_4-P_2W_{15}** and **Dy_2Mn_4-P_2W_{15},** which were experimentally explored by ^{1}H NMR longitudinal and transverse relaxivity studies. The improved relaxation ability of the POM with four Mn^{II} and 2 Dy^{III} ions in comparison to the POM with only four Mn^{II} ions proves that relaxation behaviour can be altered by chemical and /or electronic change. This work shows that presence of the heterometallic metal centers within the same molecules is a useful strategy in developing new relaxation agents for the high magnetic field applications. The incorporation of Dy^{III} ions into POM architectures represents promising strategy for the development of high-field MRI contrast agents.

References

1. M. Harris, S. Biju, T.N. Parac-Vogt, Chem. Eur. J. **25**, 13838 (2019)
2. C.Y. Chou, M. Abdesselem, C. Bouzigues, M. Chu, A. Guiga, T.H. Huang, F. Ferrage, T. Gacoin, A. Alexandrou, D. Sakellariou, Sci. Rep. **7**, 1 (2017)
3. E. Moser, E. Laistler, F. Schmitt, G. Kontaxis, Front. Phys. **5**, 1 (2017)
4. M.E. Ladd, P. Bachert, M. Meyerspeer, E. Moser, A.M. Nagel, D.G. Norris, S. Schmitter, O. Speck, S. Straub, M. Zaiss, Prog. Nucl. Magn. Reson. Spectrosc. **109**, 1 (2018)
5. G. Giovannetti, A. Guerrini, P.A. Salvadori, Magn. Reson. Imaging **34**, 730 (2016)
6. L.D. Hall, T.A. Carpenter, Magn. Reson. Imaging **10**, 713 (1992)
7. P. Caravan, Chem. Soc. Rev. **35**, 512 (2006)
8. X.Y. Zheng, J. Pellico, A.A. Khrapitchev, N.R. Sibson, J.J. Davis, Nanoscale **10**, 21041 (2018)
9. E. Debroye, S. Laurent, L. Vanderelst, R.N. Muller, T.N. Parac-Vogt, Chem. Eur. J. **19**, 16019 (2013)
10. M. Bottrill, L. Kwok, N.J. Long, Chem. Soc. Rev. **35**, 557 (2006)
11. J. Wahsner, E.M. Gale, A. Rodríguez-Rodríguez, P. Caravan, Chem. Rev. **119**, 957 (2019)
12. M.W. Marashdeh, B. Ababneh, O.M. Lemine, A. Alsadig, K. Omri, L. El Mir, A. Sulieman, E. Mattar, Results Phys. **15**, 102651 (2019)
13. G. Guthausen, J.R. Machado, B. Luy, A. Baniodeh, A.K. Powell, S. Krämer, F. Ranzinger, M.P. Herrling, S. Lackner, H. Horn, Dalton Trans. **44**, 5032 (2015)
14. J.R. Machado, A. Baniodeh, A.K. Powell, B. Luy, S. Krämer, G. Guthausen, ChemPhysChem **15**, 3608 (2014)
15. M. Ibrahim, S. Krämer, N. Schork, G. Guthausen, Dalton Trans. **48**, 15597 (2019)
16. D.-L. Long, R. Tsunashima, L. Cronin, Angew. Chem. Int. Ed. **49**, 1736 (2010)
17. M. Ibrahim, V. Mereacre, N. Leblanc, W. Wernsdorfer, C.E. Anson, A.K. Powell, Angew. Chem. Int. Ed. **54**, 15574 (2015)
18. M. Ibrahim, Y. Lan, B.S. Bassil, Y. Xiang, A. Suchopar, A.K. Powell, U. Kortz, Angew. Chem. Int. Ed. **50**, 4708 (2011)
19. A. Bijelic, M. Aureliano, A. Rompel, Angew. Chem. Int. Ed. **58**, 2980 (2019)
20. M.J. Martínez-Pérez, O. Montero, M. Evangelisti, F. Luis, J. Sesé, S. Cardona-Serra, E. Coronado, Adv. Mater. **24**, 4301 (2012)
21. S.T. Zheng, G.Y. Yang, Chem. Soc. Rev. **41**, 7623 (2012)
22. O. Oms, A. Dolbecq, P. Mialane, Chem. Soc. Rev. **41**, 7497 (2012)
23. C. Boskovic, Acc. Chem. Res. **50**, 2205 (2017)
24. X. Ma, W. Yang, L. Chen, J. Zhao, CrystEngComm **17**, 8175 (2015)
25. S. Reinoso, Dalton Trans. **40**, 6610 (2011)
26. P. Mialane, A. Dolbecq, F. Sécheresse, Chem. Commun. (2006). https://doi.org/10.1039/B603594A
27. C.J. Gómez-García, J.J. Borrás-Almenar, E. Coronado, L. Ouahab, Inorg. Chem. **33**, 4016 (1994)
28. M. Ibrahim, E. Moreno-pineda, T. Bergfeldt, C.E. Anson, A.K. Powell, Materials (Basel) **11**, 155 (2018)
29. M. Ibrahim, I.M. Mbomekallé, P. De Oliveira, A. Baksi, A.B. Carter, Y. Peng, T. Bergfeldt, S. Malik, C.E. Anson, ACS Omega **4**, 21873 (2019)
30. P. Yin, D. Li, T. Liu, Chem. Soc. Rev. **41**, 7368 (2012)
31. I. Bertini, C. Luchinat, G. Parigi, *Solution NMR of Paramagnetic Molecules: Applications to Metallobiomolecules and Models,* vol. 2 (Elsevier, Amsterdam, 2001)
32. D. Ni, W. Bu, E.B. Ehlerding, W. Cai, J. Shi, Chem. Soc. Rev. **46**, 7438 (2017)

Publisher's Note Springer Nature remains neutral with regard to jurisdictional claims in published maps and institutional affiliations.

Affiliations

Masooma Ibrahim[1] · Thomas Rudszuck[2] · Banan Kerdi[3] · Steffen Krämer[3] · Gisela Guthausen[2,4] · Annie K. Powell[1,5] ⓘ

[1] Karlsruhe Institute of Technology (KIT), Institute of Nanotechnology (INT), Hermann-von-Helmholtz-Platz 1, 76344 Eggenstein-Leopoldshafen, Germany

[2] Karlsruhe Institute of Technology (KIT), MVM-VM, Adenauerring 20b, 76131 Karlsruhe, Germany

[3] Laboratoire National des Champs Magnétiques Intenses, LNCMI-CNRS (UPR3228), EMFL, Univ. Grenoble Alpes, INSA Toulouse, Univ. Toulouse Paul Sabatier, B.P. 166, 38042 Grenoble Cedex, France

[4] Karlsruhe Institute of Technology (KIT), EBI-WCWT, Adenauerring 20b, 76131 Karlsruhe, Germany

[5] Institute of Inorganic Chemistry, Karlsruhe Institute of Technology (KIT), Engesserstrasse 15, 76131 Karlsruhe, Germany